Precision Agriculture, 6, 359–378, 2005

Evaluation of Digital Photography from Model Aircraft for Remote Sensing of Crop Biomass and Nitrogen Status

E. RAYMOND HUNT JR. erhunt@hydrolab.arsusda.gov
USDA ARS Hydrology and Remote Sensing Laboratory, Beltsville Agricultural Research Center, Building 007 Room 104, 10300 Baltimore Avenue, 20705, Beltsville, MD, USA

MICHEL CAVIGELLI
USDA ARS Sustainable Agricultural Systems Laboratory, Beltsville Agricultural Research Center, Building 001 Room 245, 10300 Baltimore Avenue, 20705, Beltsville, MD, USA

CRAIG S. T. DAUGHTRY, JAMES MCMURTREY III, AND CHARLES L. WALTHALL
USDA ARS Hydrology and Remote Sensing Laboratory, Beltsville Agricultural Research Center, Building 007 Room 104, 10300 Baltimore Avenue, 20705, Beltsville, MD, USA

Abstract. Remote sensing is a key technology for precision agriculture to assess actual crop conditions. Commercial, high-spatial-resolution imagery from aircraft and satellites are expensive so the costs may outweigh the benefits of the information. Hobbyists have been acquiring aerial photography from radio-controlled model aircraft; we evaluated these very-low-cost, very high-resolution digital photography for use in estimating nutrient status of corn and crop biomass of corn, alfalfa, and soybeans. Based on conclusions from previous work, we optimized an aerobatic model aircraft for acquiring pictures using a consumer-oriented digital camera. Colored tarpaulins were used to calibrate the images; there were large differences in digital number (DN) for the same reflectance because of differences in the exposure settings selected by the digital camera. To account for differences in exposure a Normalized Green–Red Difference Index [(NGRDI = (Green DN − Red DN)/(Green DN + Red DN)] was used; this index was linearly related to the normalized difference of the green and red reflectances, respectively. For soybeans, alfalfa and corn, dry biomass from zero to 120 g m^{-2} was linearly correlated to NGRDI, but for biomass greater than 150 g m^{-2} in corn and soybean, NGRDI did not increase further. In a fertilization experiment with corn, NGRDI did not show differences in nitrogen status, even though areas of low nitrogen status were clearly visible on late-season digital photographs. Simulations from the SAIL (Scattering of Arbitrarily Inclined Leaves) canopy radiative transfer model verified that NGRDI would be sensitive to biomass before canopy closure and that variations in leaf chlorophyll concentration would not be detectable. There are many advantages of model aircraft platforms for precision agriculture; currently, the imagery is best visually interpreted. Automated analysis of within-field variability requires more work on sensors that can be used with model aircraft platforms.

Keywords: radio-controlled model aircraft, color imagery, remote sensing, biomass, nutrient status, Normalized Green–Red Difference Index

Introduction

There is a high potential for remote sensing to be used operationally in precision agriculture (Lu *et al.*, 1997; Moran *et al.*, 1997; Pierce and Nowak, 1999; Barnes

et al., 2003; Pinter *et al*., 2003). However, the adoption of remote sensing by farmers is limited by training, costs, and timely availability of imagery (Robert, 2002). Satellite and airborne sensors either have high cost and high spatial resolution (sufficient for precision agriculture) or low cost and low spatial resolution (Hunt *et al*., 2002, 2003a). Satellite data may have all of the important attributes for precision agriculture, but may not be useful because of cloud cover during acquisition.

Crop nutrient requirements can be estimated from chlorophyll concentration and biomass can be estimated from Leaf Area Index (LAI), both of which can be remotely sensed (Bausch and Duke, 1996; Blackmer *et al*., 1996b; Daughtry *et al*., 2000; Scharf *et al*., 2002; Doraiswamy *et al*., 2003). Sensors do not have to be technologically advanced; aerial photography with either color or color-infrared film is useful for mapping out biomass and nitrogen requirements (Blackmer *et al*., 1996a; Scharf and Lory, 2002; Scharf *et al*., 2002). Furthermore, platforms do not have to be sophisticated; ultralight aircraft (Clevers, 1988; Waring *et al*., 1995; Booth et al., 2003; Hunt *et al*., 2003b), blimps (Inoue *et al*., 2000), powered parasails (Moran *et al*., 2003; Lopez and Robert, 2003), and helicopters (Hongoh *et al*., 2001) have been used for high-resolution remote sensing platforms.

Quilter and Anderson (2000) suggested that aerial photography from radio-controlled model aircraft can provide very-low-cost, very-high-resolution imagery. Photographic imagery acquired from model-aircraft platforms have substantially lower cost for a given spatial resolution compared with airborne and satellite sensors (Hunt *et al*., 2002). Hunt *et al*. (2002, 2003a) used color-infrared film with a low-cost automatic camera and found the Normalized Difference Vegetation Index (NDVI) from the model aircraft was comparable with NDVI from advanced sensors. Some of the problems encountered in the preliminary work were film overexposure, lack of spectral and radiometric calibration, and the need to have long take-off and landing areas (Hunt *et al*., 2003a).

Radio-controlled model aircraft show promise as a low-cost platform for remote sensing; however, more work is required to optimize the system for operational use. Because of the spectral differences between vegetation and soil at green and red wavelengths, we hypothesized color imagery would also be useful for determining both biomass and nutrient status, allowing the use of light-weight digital cameras. We also made further improvements to a fixed-wing model aircraft to test its usefulness as a remote sensing platform for precision agriculture.

Materials and methods

Model aircraft

Different types of model aircraft have different capabilities, any one of which can be advantageous or disadvantageous under different circumstances (Hunt *et al*., 2002, 2003a). Compromises must be made among ease of flying, stability in wind, handling flight failures, distance covered, and takeoff/landing requirements. Aerobatic model aircraft can be flown from mowed, grassy fields and require shorter distances for takeoff and landing compared to other fixed-wing aircraft. We used an Edge 540T

fixed wing aircraft (Aeroworks, Inc., Aurora, CO, USA) with a 20-cm^3 two-stroke engine (Webra Mode1lmotoren, AG, Enzeafeld, Austria) and JR electric servo motors (Horizon Hobbies, Champaign, IL, USA), JR radio transmitters, and JR receivers (Figure 1(a)).[1] The model aircraft was modified to reduce mass by removing some redundant structural material and to increase strength by using carbon–fiber-composite replacement parts. The engine muffler was mounted to vent exhaust above the plane, so that the oily exhaust would not deposit residue on the bottom of the fuselage. We constructed a balsa wood box and mounted the box onto the fuselage bottom to hold a camera in place (Figure 1(b)). A JR electric servo motor was attached to the box, which pressed the camera shutter-release button under control by the radio transmitter (Figure 1(b)).

Flights were generally made between 0930 and 1130 h, Eastern Daylight Time, as a compromise between wind speed and solar elevations. High solar elevations reduce

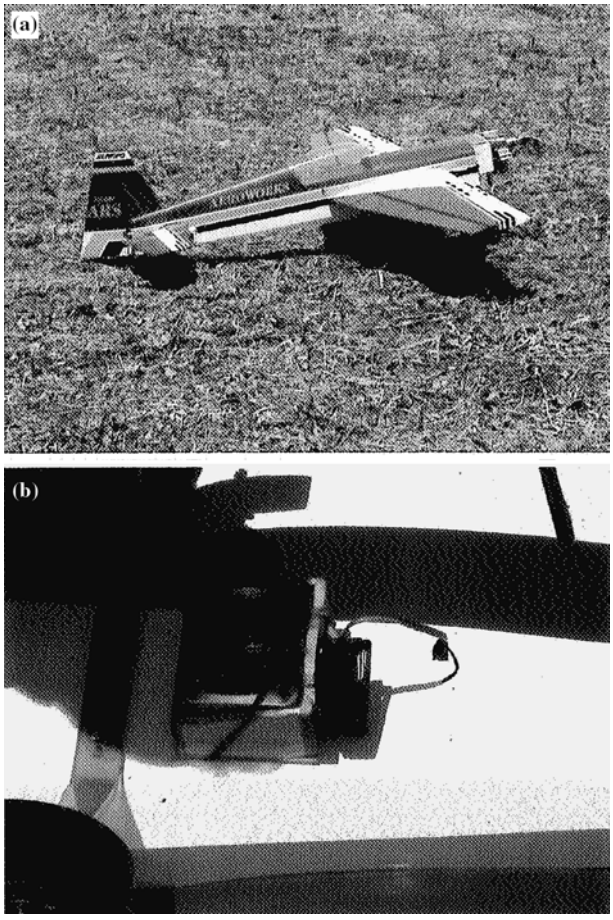

Figure 1. (a) Radio controlled model aircraft with 1.52 m length and 1.65 m wingspan. (b) Digital camera mounted on the bottom of the aircraft fuselage.

the amount of shadow in an image and early mornings had still wind conditions, with the wind speeds increasing over the day. It would generally take about 45 min after arrival to set up the airplane, fly the field, examine the images, and pack up.

Remote sensing

We used an Olympus D40 4.1-megapixel color digital camera (Olympus, Inc., Melville, NY, USA). The shutter speed was set at 0.001 s, and the aperture was adjusted by the camera to control light intensity. The lens was set to be wide angle with the focus distance set at infinity. At an altitude of about 200 m, several plots could be covered in one picture, with a pixel size of about 100 mm. After the plane landed, images from the digital camera were immediately downloaded into a laptop computer and examined, so that spatial coverage of the photographs could be determined.

The digital pictures (JPEG format) were opened with the ENVI image processing software (Research Systems, Inc., Boulder, CO, USA). The mean digital numbers for the red, green and blue bands of each plot were determined by including the pixels into a "region of interest," and using the statistical tools in ENVI.

Radiometric and spectral calibration

Exposure settings on the digital camera are selected based on overall light intensity, which varies over time because of changes in solar elevation, atmospheric transmittance and clouds (Gates, 1980). Radiometric calibration of digital numbers to reflectances corrects for these changes. The original idea was to use colored tarpaulins to calibrate the digital photographs to red, green and blue reflectances (Moran *et al.*, 2003). However, the camera's field of view was sufficiently small to prevent having the tarpaulins in each photograph, and the camera's exposure settings varied with each aerial photograph, so the calibration determined for one photograph could not be used for another photograph.

Five colored tarpaulins (beige, gray, green, red, and black) were used to test the camera's spectral calibration. The spectral bidirectional reflectance factors of the tarpaulins were determined under sunlight using an ASD FR Pro spectroradiometer (Analytical Spectral Devices, Inc., Boulder, CO, USA) and a Spectralon reference panel (Labsphere, Inc., North Sutton, NH, USA).

The wavelengths covered by each band of the digital camera were not available from the manufacturer. We used the monochromatic light source from a SPEX 1680 Double Spectrometer (HORIBA Jobin Yvon, Inc., Edison, NJ, USA) and took photographs of the light output from 400 to 700 nm at 10-nm intervals. The light source intensity was balanced to match the spectral distribution of sunlight (James McMurtrey, Maryn Butcher, and Larry Corp, personal communication). This procedure was replicated twice. The digital numbers were obtained from two locations around the 2 mm slit in each photograph. Digital numbers for each wavelength (DN_λ) from 400 to 700 nm were obtained from linear interpolation for each 10-mm

interval. Weighted reflectances of the tarpaulins for the red, green and blue bands (R_{band}) were calculated:

$$R_{band} = \sum R_\lambda DN_\lambda \Big/ \sum DN_\lambda \quad \text{for } \lambda \text{ from 400 to 700 nm} \tag{1}$$

where R_λ is the spectral reflectance at wavelength λ.

Normalized Green–Red Difference Index

Topography (slope and azimuth) affects the surface irradiance (Gates, 1980), so different areas within an image with the same surface reflectance will have difference digital numbers in an image. The difference in digital numbers between near-infrared and red hands is large for vegetation and small for soils (Huete, 2004), but the absolute difference is highly sensitive to variations in irradiance. To account for within-scene and between-date variations in irradiance, Rouse *et al*. (1974) developed the Normalized Difference Vegetation Index (NDVI), in which the difference in digital numbers between the near-infrared and red bands was normalized by dividing by the sum of the bands. Whereas most consumer-oriented digital cameras have detectors that are capable of detecting near-infrared wavelengths, filters are used to prevent near infrared light from reaching the detector; hence NDVI cannot be calculated.

There are also differences between the green and red bands for vegetation and soil, although these differences are not as large as with near-infrared bands. We used the Normalized Green–Red Difference Index (NGRDI) to analyze the images from the digital camera:

$$\text{NGRDI} = (\text{Green DN} - \text{Red DN})/(\text{Green DN} + \text{Red DN}) \tag{2}$$

where Green DN and Red DN are the digital numbers of the green and red bands, respectively.

The difference between the green and red digital numbers differentiates between plants and soil, and the sum normalizes for variations in light intensity between different images. The possible range of NGRDI is from −1.0 to 1.0, but the actual variation of NGRDI is small for most targets.

This index is mathematically related other remotely sensed indices:

$$\text{NGRDI} = (\text{ratio} - 1)/(\text{ratio} + 1) \tag{3}$$

where the ratio is Green DN/Red DN, so conclusions based on the NGRDI also apply to the ratio of Green DN/Red DN.

Alfalfa biomass

Alfalfa (*Medicago sativa* L. cultivar cimarron) was planted in 2001 in field NG-1Z at Beltsville to study organic farming practices. The alfalfa was mowed for hay on July

15, 2002 and the radio-controlled model aircraft was flown on August 6, 2002. Cumulative precipitation for 2002 was 339 mm on August 6, which was 296 mm below normal (54 years of record), so there was little re-growth. Twenty-four plots were selected by eye to obtain the largest possible range of biomass, and located with a Precision Lightweight Global Positioning System Receiver (Rockwell-Collins International, Inc., Cedar Rapids, IA, USA), which has about 4-m horizontal accuracy. All plant material within a 0.25 m^2 frame was cut at soil level on August 8, 2002, dried at 60°C, and weighed. The single digital image was georegistered using 25 ground control points to an accuracy of 5 m, and 25 pixels centered on the plot position center were used to calculate the mean digital numbers of the red green and blue bands.

Corn and soybean biomass

The USDA Fanning Systems Project (FSP) at Beltsville, Maryland, is a long-term cropping systems trial designed to compare the agronomic and ecological performance of two conventional cropping systems and three organic cropping systems (http://www.ba.ars.usda.gov/sasl/research/fsp.html; last accessed November 30, 2004). Full-size farming equipment is used for all crop management operations. The soils are well-drained, moderately well-drained and somewhat poorly drained silt loam Ultisols. Corn (*Zea mays* L. cultivar Fielders Choice 95+) and soybean (*Glycine max* L. cultivar Northrup King R-366) were used to examine the relationship between NGRDI and biomass. Plot sizes were 9 m × 111 m.

Precipitation in 2003 was well above normal (Table 1), and the waterlogged soils interfered with planting crops in late May and early June. Due to the wet soil conditions, some plots were planted late June, and for crops planted early, the loss of soil nitrogen via denitrification was apparent in flooded areas. To capture a full range of crop biomass levels, 20 sampling locations in each of corn and soybean were selected by eye to obtain a large range of biomass levels from no-till, conventional till, and organic system plots. The model aircraft was flown on July 23, 2003 and biomass was measured the following day. At each location, three plants were cut at soil level arid put into plastic bags, which were sealed until their wet weights were recorded. Then, plants were transferred to cloth bags, dried at 60°C, and weighed. Plant population densities were determined at each sampling location by counting the number of plants within a 1 m radius.

The center point for each sampling location was determined by measuring the distance from two perpendicular edges of the plot, so under any oblique view from the model aircraft, the location can be determined geometrically on the image without resorting to georegistration of a large number of images. All of the pixels within a 1-m radius were used to calculate the mean digital numbers.

Corn nitrogen status

To determine when nutrient deficiency can be detected, corn (*Zea mays* L. cultivar Pioneer hybrid 111894) was planted on May 5, 2003 in field 5–8 at Beltsville, MD,

Table 1. Growth stage of corn in field 5–8 using the leaf collar method (Ritchie *et al.,* 1993)

			Cumulative precipitation (mm)		
Date	Day of year	Growth stage[a]	2003	Mean	Departure
May 5	125	Planting	313	324	−11
May 20	140	VE	389	377	12
May 30	150	V2	460	409	51
June 5	156	V4	477	433	44
June 9	160	V5	519	445	74
June 24	175	V7	616	491	125
June 30	181	V9	617	515	102
July 15	196	V14	702	561	141
July 30	211	VT	765	607	158
August 8	220	R1	778	635	143

Mean (1949–2002) and 2003 cumulative precipitation for Beltsville Agricultural Research Center are shown.

[a]V—vegetative stage with the number of the oldest leaf with a visible leaf collar, E—seed leaf emerging from soil, T—tassel emerging from stalk, R—reproductive stage.

with 20 kg N ha^{-1} starter nitrogen (Table 1). The original design was to have an early and late planting (Hunt *et al*., 2002, 2003a), but the wet weather prevented planting in late May/early June (Table 1). The modified design was a randomized complete block design with two replications of each applied nitrogen level. Each plot was 37 nm long and consisted of 48 rows of corn planted 0.76 m apart in an east–west orientation. The plot boundaries were located with a Trimble GPS Total Station 4700 Real-Time Kinematic (Trimble, Inc., Sunnyvale, CA, USA) with horizontal accuracy of 30 mm and vertical accuracy of 50 mm. Corn shoots were cut at all of the plot boundaries so each plot could be identified in an image without image georegistration.

The early planting had normal development (Table 1) with the growth stage determined by the leaf-collar method (Ritchie *et al*., 1993). Plots 1 through 4 and plots 5 through 8 were randomly assigned a nitrogen treatment (Table 2). Sidedress N was applied on July 11, 2003 at 0%, 25%, 50%, and 100% of the recommended rate of 125 kg N ha^{-1} (Table 2).

Before and after sidedress nitrogen, leaf chlorophyll concentration was measured according to Blackmer and Schepers (1995) using a Minolta SPAD-502 chlorophyll meter (Spectrum Technologies, Inc., Plainfield, IL, USA). In each plot, chlorophyll was measured on the topmost leaf with a visible leaf collar, midway from the leaf tip to the leaf collar, for every tenth plant in three different rows. A general linear model analysis of variance procedure was used to determine separability of plant parameters followed by a Student Newman–Kuels multiple range test for assessment of significant mean separations, $P \leq 0.05$ (SAS Institute, 1999).

The aircraft was flown over the held on seven dates during 2003. All of the pixels within a plot were used to obtain the mean digital numbers. Plant population density of each plot was determined by counting all of the plants in six rows evenly spaced across the plot.

Table 2. Plant density and SPAD chlorophyll-meter measurements of corn on two dates in 2003

N level %	Plot	Density (plants m^{-2})	Chlorophyll-meter	
			June 24	August 6
0	2	5.40a	34.7a,b	39.4a
0	5	5.84b	31.1b	41.8a
25	4	5.40a,b	32.8b	53.1b,c
25	6	5.36a	25.4c	50.7b
50	1	5.64a	36.7a	52.6b,c
50	8	5.47a	24.4c	49.8b
100	3	5.92b	36.1a	55.7c,d
100	7	6.03b	24.8c	58.7d

N level was fraction of 125 kg N ha^{-1} applied as sidedress. Values followed by the same letter within a column are not significantly different at $P \leq 0.05$ using a Student Newman–Kuels multiple range test.

SAIL canopy model analyses

Because the use of NGRDI is not well established for vegetation remote sensing, we used the Scattering by Arbitrarily Inclined Leaves (SAIL) model to predict canopy reflectances for various LAI (Verhoef, 1984). The SAIL model is now used to prototype vegetation indices before testing in the field and to invert spectral reflectances to biophysical parameters (Zarco-Tejada *et al.*, 2003). Spectral reflectances and transmittances of the upper-most, fully expanded corn leaves from the nutrient experiment were measured with the ASD spectroradiometer and a LI-1800-12 integrating sphere (LI-COR, Inc., Lincoln, NE, USA). Spectral reflectance of the soil in the field was measured with the ASD spectroradiometer. We used other SAIL model parameters, particularly the leaf angle distribution, from Daughtry *et al.* (2000).

Results and discussion

Aerial photography

The images acquired from the radio-controlled model aircraft were generally in good focus and had good contrast (Figure 2). It was somewhat difficult to get pictures centered over the various fields, but during the average of 8–10 min of flying time, many pictures were taken by the digital camera. Video anal timed picture modes were also available with this camera, but these modes did not provide any advantages. Each usable picture required visible ground control points or plot boundaries so the location could be determined. If none of the pictures covered the area on initial inspection, the field was re-flown. Sudden changes in aircraft position due to wind can be seen as blurriness in some pictures (for example Figure 2(b)), which were evident only upon close inspection of the image.

The aerobatic model aircraft had superior performance in takeoff and landings, which allowed overflights of more fields compared to the trainer model aircraft used

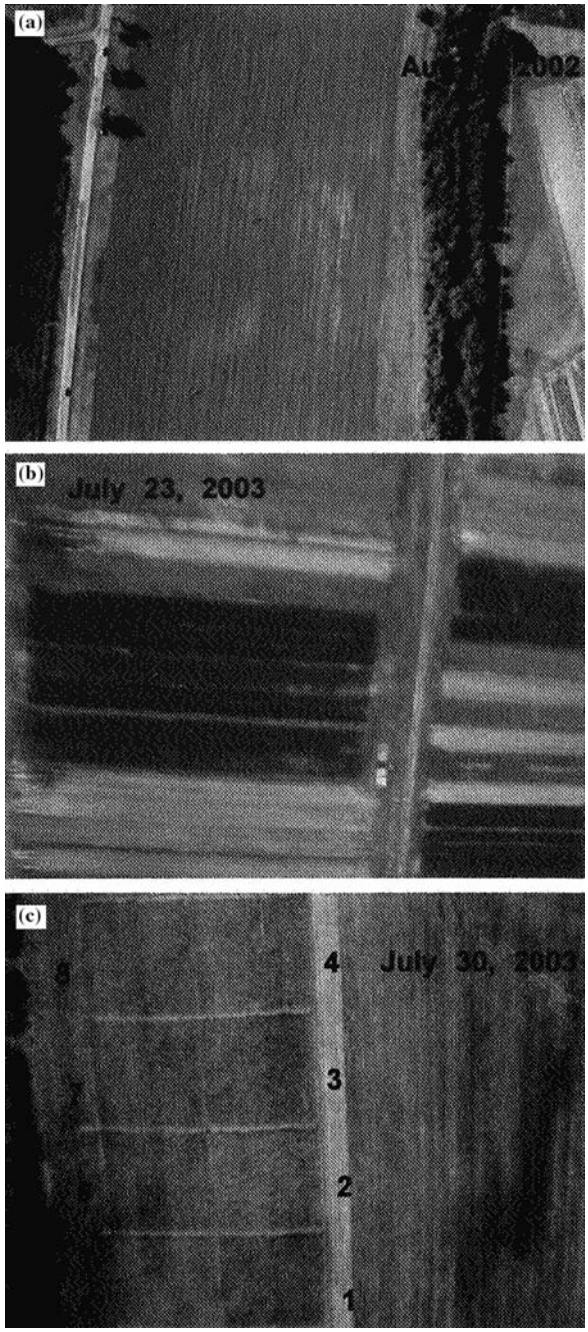

Figure 2. Digital color images acquired the radio-controlled model aircraft. (a) Field NG-1Z with alfalfa (August 8, 2002). (b) Farming Systems Project with both corn and soybean plots (July 23, 2003); and (c) field 5–8 with an applied nitrogen experiment (July 30, 2003). In b, the colored tarpaulins (2.85 m × 2.85 m) were used for camera calibration. In c, the plot numbers are shown.

by Hunt *et al*. (2002, 2003a). The field NG-1Z was flown by both aircraft, but alfalfa was only grown there in 2002, so the two systems could not be compared over the same target. The Farming Systems Project fields (corn and soybean biomass) and field 5–8 (corn nutrient status) could not have been flown by the trainer aircraft used by Hunt *et al*. (2002, 2003a), because suitable takeoff and landing areas were not available. However, the trainer model aircraft had more stability in the air and required less expertise to fly.

The images in Figure 2 were also much improved over the initial attempts with a low-cost automatic camera and color-infrared film (Hunt *et al*., 2002, 2003a). Most of the reason for the better imagery was the short exposure time (0.001 s). High-quality, high-cost automatic film cameras generally have internal, near-infrared sensors, which may expose color-infrared film. Furthermore, the low-cost cameras set the film speed to ISO 100, whereas the actual speed of the color-infrared film was ISO 200, therefore overexposing the color-infrared film (Hunt *et al*., 2002, 2003a). Another advantage we found for the digital camera was that the images were examined right after landing, which ensured the entire field was covered, whereas color-infrared film had to be developed.

It is feasible to adapt digital color cameras with near-infrared filters (Yang *et al*., 2000; Milton, 2002), but it is difficult to mount these modified cameras onto model aircraft. Four-band sensors with a near-infrared band, are generally much heavier and require external power; therefore are not yet suitable for radio-controlled model aircraft.

Radiometric and spectral calibration

The spectral reflectances at visible wavelengths of each tarpaulin corresponded closely with the color of the five tarpaulins (Figure 3). The spectral sensitivity of the digital camera (Figure 4) generally matched the spectral sensitivity of the normal human eye (Wald, 1968). One notable exception was that the red band of the digital camera was sensitive to blue wavelengths (Figure 4), hence pictures of object at 425 nm would appear to be more purple rather than violet.

Using the definition of the red color as the mean reflectance from 600 to 700 nm, then the red-band reflectance of the red tarpaulin was 45%. However, taking the red spectral sensitivity of the human eye to be from 580 to 650 nm (Wald, 1968), the red-band reflectance was 30%. Using the typical remote sensing definition of spectral sensitivity as the wavelengths at 50% of maximum response, the wavelength range of the red band was 580–660 nm, so the red reflectance was 33%. Using the weighted spectral response of the digital camera (Eq. (1)), the mean red reflectance was only 25% for the red tarpaulin. The weighted green reflectance of the green tarpaulin was 20%. The weighted green and red reflectances for the beige tarpaulin were 27% and 29%, respectively.

About half of the images of the colored tarpaulins (see Figure 2(b)) had mean digital numbers greater than 250 for the green and red bands of the green, red, and beige tarpaulins, indicating the camera detector was light saturated due to the high-weighted reflectances. For these cases, the data for the tarpaulins were not analyzed further; however, other areas in these images were generally not light saturated and

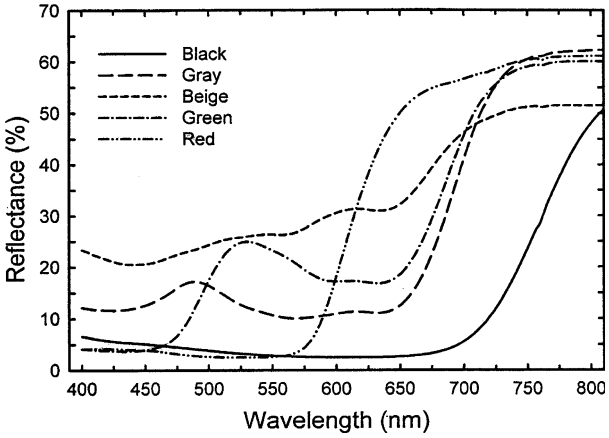

Figure 3. Spectral reflectances of five colored tarpaulins.

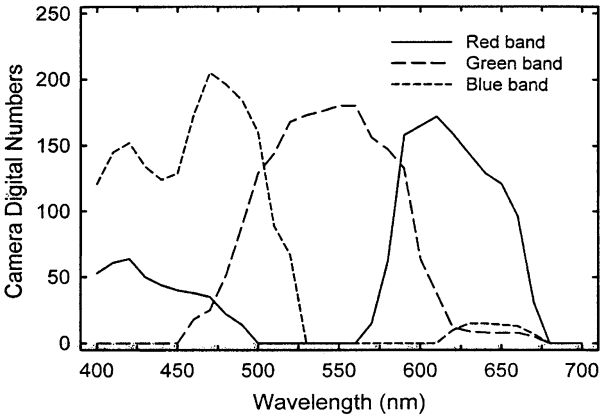

Figure 4. Spectral response of the digital camera's red, green and blue bands. The monochromatic light source was adjusted to simulate the daylight spectrum.

contained useful data. For the remaining images of the colored tarpaulin, there was a linear relationship between the digital numbers and the weighted reflectances for each band (data not shown). Because the camera aperture changed with changing light level, the slope and intercept for a single image differed considerably from the other images. Thus, the regression coefficients between digital numbers and reflectances could not be used to calibrate the digital numbers to reflectances even for adjacent images, necessitating an alternative method of radiometric calibration.

Normalized indices such as the NGRDI were designed to reduce variation caused by differences in irradiance and exposure. Mean digital numbers of the red and green bands were used to calculate NGRDI for each tarpaulin in the images. There was a linear relationship between the camera NGRDI and the NGDRI calculated for the five colored tarpaulins from the weighted reflectances (Figure 5). Whereas the regression slope and intercept were significantly different from 1.0 and 0.0, respec-

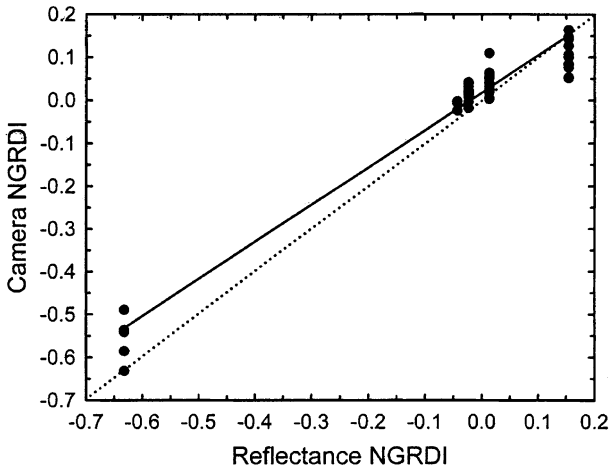

Figure 5. Comparison of the Normalized Green–Red Difference Index for five colored tarpaulins between camera digital numbers and weighted spectral reflectances. The solid line is a least-squares regression (Camera NGRDI = 0.018 + 0.87 reflectance NGRDI, $R^2 = 0.96$, se($\hat{y}$) = 0.037, $P < 0.00001$) and the dotted line is the 1:1 line. The intercept is significantly different from 0.0 [95% confidence interval = (0.0073, 0.023)] and the slope is significantly different from 1.0 [95% confidence interval = (0.82, 0.92)]. Data were used only when the digital numbers <2.50.

tively, the data fell very close to the 1:1 line (Figure 5). Therefore, NGRDI from the digital numbers were sufficiently close to the values calculated from the reflectances to be used without further radiometric calibration.

NGRDI and biomass

For alfalfa, corn, and soybean, NGRDI were linearly related to biomass levels up to about 120 gm^{-2} (Figures 6–8). At higher levels of biomass for corn and soybean, NGRDI was saturated at a maximum value, which averaged 0.05 for corn and 0.13 for soybean, respectively (Figures 7 and 8). The maximum amount of biomass in the alfalfa field was low (Figure 6), hence no saturation of NGRDI was observed.

Corn nitrogen status

Early in the season, there were significant differences among the 8 plots in mean chlorophyll content (Table 2). Plots 1–3 had the relative highest elevation (34.5 m) as determined by global positioning system data, plots 4 and 5 had intermediate elevation (34.0 m), and plots 6–8 had the lowest elevation (33.6 m) and were frequently flooded in 2003. The low chlorophyll contents of plots 6–8 reflected the low nitrogen status. After sidedress nitrogen was applied, mean chlorophyll content was related to application rate for the 0% and 100% treatments (Table 2). There was no significant difference in mean chlorophyll content between the 25% and 50% nitrogen treatments after application of sidedress nitrogen, but tile chlorophyll contents were intermediate between the 0% and 100% treatments (Table 2).

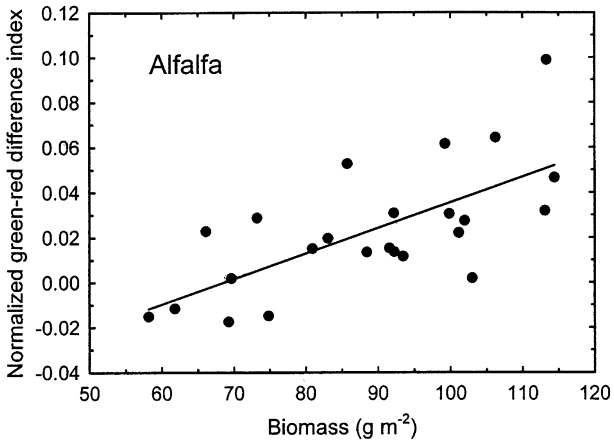

Figure 6. Normalized Green–Red Difference Index versus biomass for alfalfa on August 8, 2002. The solid line is a regression (NGRDI = −0.078 + 0.0011 biomass, R^2 = 0.47, se($\hat{y}$) = 0.021, P = 0.00024).

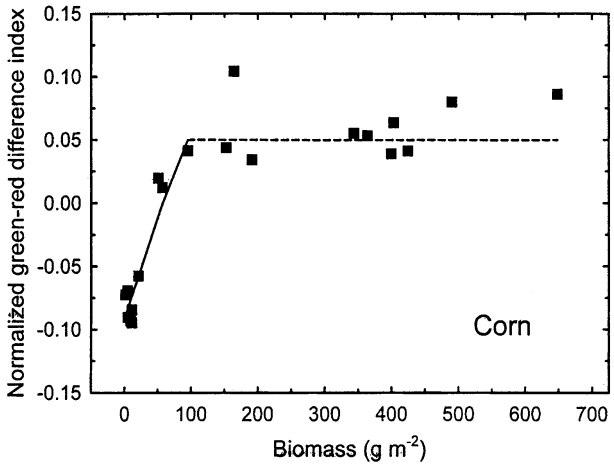

Figure 7. NGRDI versus corn biomass at FSP fields on July 23, 2003. The solid line at low biomass is a regression (NGRDI = −0.091 + 0.0016 biomass, R^2 = 0.88, se($\hat{y}$) = 0.019, P = 0.00015) and the dashed line at high biomass is the mean of NGRDI.

NGRDI started out at a low level, about −0.03, from emergence through the V2 growth stage (Figure 9, Table 1). In July, NGRDI reached maximum value of 0.02 (Figure 9). In May, soils were wet and dark, so the difference between Green DN and Red DN was small for all plots. Large differences in NGRDI among plots were seen from late June through the beginning of August (Figure 9). There were small but significant differences in plant density among the plots (Table 2), which was not correlated with NGRDI on any date (Figure 9).

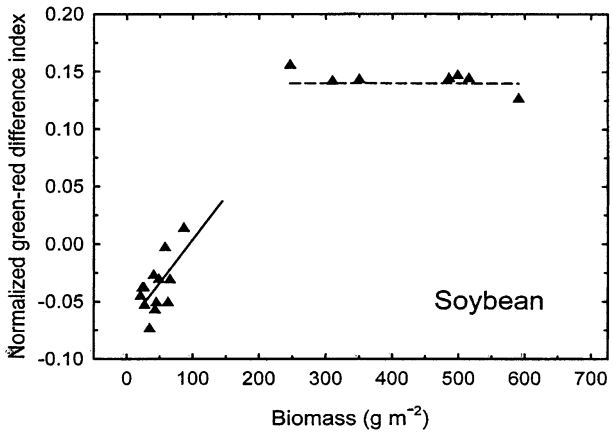

Figure 8. NGRDI versus soybean biomass at FSP fields on July 23, 2003. The solid line at low biomass is a regression (NGRDI = −0.071 + 0.00075 biomass, R^2 = 0.39, se($\hat{y}$) = 0.018, P = 0.022) and the dashed line at high biomass is the mean NGRDI.

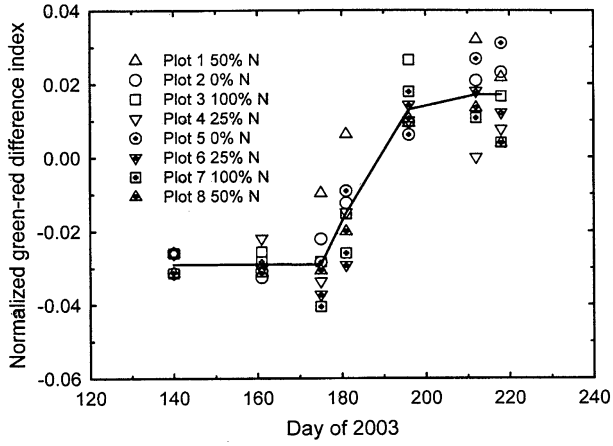

Figure 9. Changes of NGRDI over the 2003 growing season for corn fertilization experiment. The lines indicate the changes of mean NGRDI for the 8 plots.

On June 24, there was a significant positive correlation between mean chlorophyll content and NGRDI. The 95% confidence interval for the regression intercept was (−0.074, −0.069), the 95% confidence interval for the regression slope was (0.0004, 0.0024), the goodness-of-fit (R^2) was 0.56, and the probability (P) that the null hypothesis was 0.033, with only 6 degrees of freedom. However, on August 6, the correlation between chlorophyll content and NGRDI was not significant with a P = 0.063. Because NGRDI is based on the green and red reflectances, it was expected that there would be a strong positive relationship with chlorophyll content on both dates.

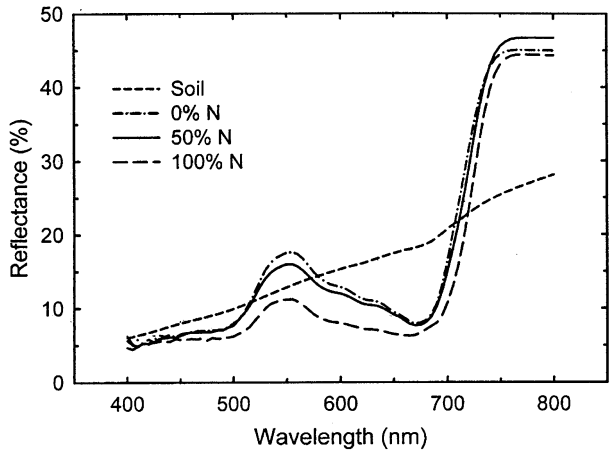

Figure 10. Reflectance of soil and corn leaves at three levels of applied nitrogen. These data were used as inputs to the Scattering by Arbitrarily Inclined Leaves (SAIL) canopy reflectance model.

SAIL model analyses

Reflectances of individual corn leaves decreased at both green and red wavelengths with increasing amounts of applied nitrogen (Figure 10). The differences among leaf reflectances were largest around 550 nm wavelength in the green, and were smallest around 680 nm wavelength near the chlorophyll absorption maximum (Figure 10). However, there was no spectral response of the digital camera to radiation at 680 nm, and both the red and green bands were sensitive to radiation at 580 nm (Figure 4). Thus, leaf NGRDI based on weighted reflectances was about 0.05 for the three treatments. For dry soil, NGRDI was about −0.20 using weighted reflectances (Figure 10). When the reflectance data were used as inputs to the SAIL model, the canopy reflectance spectra were dominated by soil at low LAI and by the leaves at high LAI (Figure 11). NGRDI calculated using weighted reflectances for the red and green bands varied from about −0.20 at lowest LAI to about 0.05 at an LAI of 5.0 (Figure 12). Significantly, NGRDI was saturated above an LAI of 2 and there were essentially no differences in NGRDI among nitrogen treatments (Figure 12).

Biomass and LAI are usually highly correlated during early crop growth, so the SAIL model simulations agreed with the observations of NGRDI at low biomass for alfalfa (Figure 6), corn (Figure 7), and soybean (Figure 8). Similarly, at high biomass, the SAIL model simulations agreed with the observations that NGRDI was saturated for corn (Figure 7) and soybean (Figure 8).

The simulations with the SAIL model indicated that there should be no response of NGRDI to differences in chlorophyll content, based on the spectral sensitivity of the digital camera. Chlorophyll content was positively correlated with NGRDI on the June 24 overflight but not for the August 6 overflight. Generally, the growth rate and chlorophyll concentration in corn is correlated with soil nitrogen concentration. Early in the growing season when biomass was less than 100 g m^{-2}, areas with high

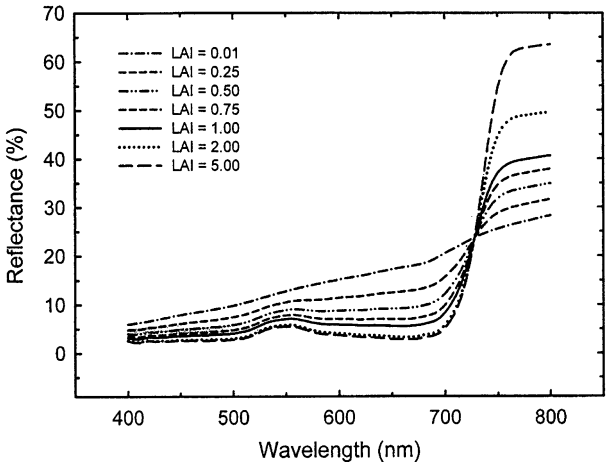

Figure 11. Simulated canopy reflectances from the SAIL model at various Leaf Area Index (LAI) for corn with 100% of the applied nitrogen fertilizer. Simulations from the SAIL model for 50% and 0% applied nitrogen show similar trends.

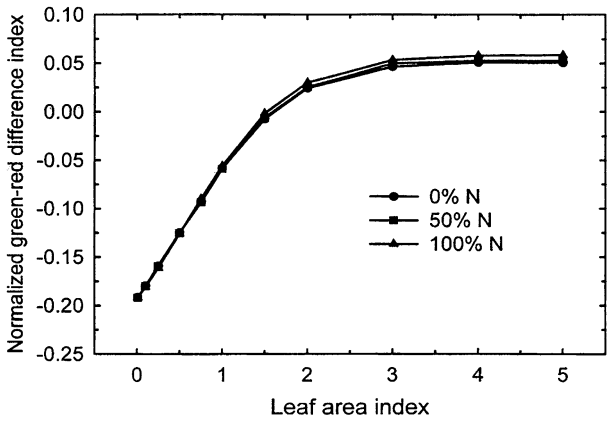

Figure 12. SML model simulations of Normalized Green–Red Difference Index for corn at various Leaf Area Index (LAI) at three levels of applied nitrogen.

soil nitrogen concentration would have had higher biomass and chlorophyll concentration. Whereas biomass was not measured in this experiment, it is reasonable to conclude the correlation between NGRDI with chlorophyll content on the June 24 overflight was due to an underlying correlation with biomass (Figure 9).

In Figure 2c, plots 2 and 5 (0% applied sidedress N) were distinguishable from the other plots in the image, because these plots were more yellow–green. The yellow green color was from increased digital numbers in both the red and green bands. The simulations with the SAIL model show that the mean canopy reflectance over the entire visible range of 400–650 nm decreased with increasing applied nitrogen, but only when NGRDI was saturated at high LAI (Figure 13). Whereas colors are

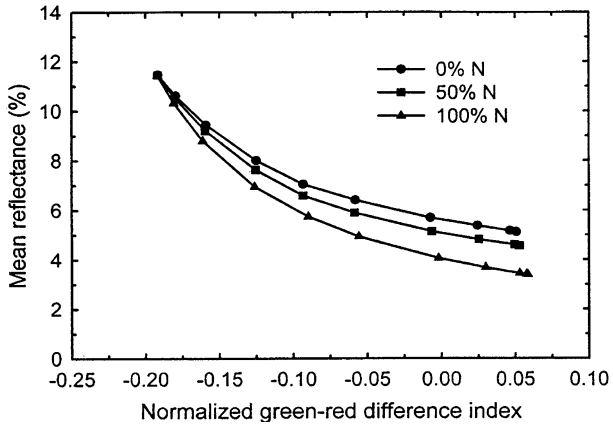

Figure 13. SAIL model simulations of mean visible reflectance for corn at various NGRDI at three applied nitrogen levels. Mean reflectance is the average from 400 to 661 nm wavelength. Variations in NGRDI were obtained from variation in Leaf Area Index (LAI).

usually defined in terms of red, green and blue reflectances, color as perceived by humans is also defined in terms of hue, saturation and intensity (Shevell, 2003). Low chlorophyll contents are related to an increase in intensity, which is indicated by greater mean visible reflectances for a given NGRDI (Figure 13). Therefore, areas of low nitrogen in Figure 2(c) were distinguished visually by the shift in intensity. If the red band of the digital camera was shifted to longer wavelength (around 680 nm), then NGRDI would be more sensitive to differences in chlorophyll concentration.

A single index, such as the NGRDI, is sensitive to many canopy factors, primarily the amount of vegetation because of the spectral differences between vegetation and soil (Daughtry *et al.*, 2000). Two or more remote-sensing indices have to be combined to identify areas of low chlorophyll concentrations simultaneously with changes in vegetation biomass (Daughtry *et al.*, 2000). Because color digital cameras have only three bands, automated determination of multiple canopy factors (both biomass and nutrient status) from a single image is not feasible. Instead, the pictures would have to visually interpreted based on qualitative judgments in order to get the maximum amount of information from aerial photographs using a consumer-oriented digital camera.

Conclusions

This study was a comprehensive examination on the use of radio-controlled model aircraft and digital cameras as a very-low-cost, very-high-spatial-resolution alternative for remote sensing in precision agriculture. The results were mixed, because there were limitations imposed by the use of fixed-wing model aircraft and there were limitations imposed by the use of a consumer-oriented digital camera. The maximum amount of information would be obtained from visual interpretation of the images, particularly regarding crop nitrogen status. Automated digital image processing based on indices usually removes some of the subjectivity involved with interpreta-

tion, and hence is an important step in exacting useable information from the imagery. We are not advocates stating the technologies used in this study are a panacea for precision agriculture. On the whole, the use of model aircraft and digital cameras overcame many of the problems associated with commercial satellite and airborne imagery, thus these technologies warrant continued investigation and improvement. Based on the development of sophisticated, lightweight sensors used in unmanned airborne vehicles (UAVs) for military operations, major advances using model aircraft or other alternative platforms for remote sensing in precision agriculture should be expected.

Acknowledgments

First, we thank Jonathan Baker for building and flying the radio-controlled model aircraft. The initial work on use of radio-controlled model aircraft for precision farming was done with a summer program of science, mathematics and engineering, called Imago Excellence/E1 Ingeniero, for seventh and eighth grade Hispanic students at the Beltsville Agricultural Research Center (BARC) led by Ms. Lucy Negrón-Evelyn. Also, we thank John Schroeder, Anne Conklin, Larry Corp, Maryn Butcher and BARC Farm Operations for their assistance.

Note

1. Mention of commercial products are for information only and do not constitute an endorsement by the USDA Agricultural Research Service.

References

Barnes, E. M., Sudduth, K. A., Hummel, J. W., Lesch, S. M., Corwin, D. L., Yang, C., Daughtry, C. S. T. and Bausch, W. C. 2003. Remote- and ground-based sensor techniques to map soil properties. Photogrammetric Engineering & Remote Sensing **69**(6), 619–630.

Bausch, W. C. and Duke, H. R. 1996. Remote sensing of plant nitrogen status in corn. Transactions of the ASAE **39**, 1869–1875.

Blackmer, T. M. and Schepers, J. S. 1995. Use of a chlorophyll meter to monitor nitrogen status and schedule fertilization for corn. Journal of Production Agriculture **8**, 56–60.

Blackmer, T. M., Schepers, J. S., Varvel, G. E. and Meyer, G. E. 1996a. Analysis of aerial photography for nitrogen stress within corn fields. Agronomy Journal **88**, 729–733.

Blackmer, T. M., Schepers, J. S., Varvel, G.E. and Walter-Shea, E. A. 1996b. Nitrogen deficiency detection using reflected shortwave radiation from irrigated corn canopies. Agronomy Journal **88**, 1–5.

Booth, D. T., Glenn, D., Keating, B., Nance, J., Cox, S. E. and Barriere J. P. 2003. Monitoring rangeland watersheds with very-large scale aerial imagery. In: *Proceedings of the First Interagency Conference on Research in the Watersheds*, edited by Kenneth G. Renard (USDA-ARS, Washington, DC), pp. 212–215.

Clevers, J. G. P. W. 1988. Multispectral aerial photography as a new method in agricultural field trial analysis. International Journal of Remote Sensing **9**(2), 319–332.

Daughtry, C. S. T., Walthall, C. L., Kim, M. S., de Brown Colstoun, E. and McMurtrey, J. E. 2000. Estimating corn leaf chlorophyll concentration from leaf and canopy reflectance. Remote Sensing of Environment **74**, 229–239.

Doraiswamy, P. C., Moulin, S., Cook, P. W. and Stern, A. 2003. Crop yield assessment from remote sensing. Photogrammetric Engineering & Remote Sensing **69**(6), 665–674.

Gates, D. M. 1980. *Biophysical Ecology*. (Springer-Verlag, New York, USA).

Hongoh, D., Kajiwara, K. and Honda, Y. 2001. Developing ground truth measurement system using RC helicopter and BRDF model in forest area. In *Proceedings of the 22nd Asian Conference on Remote Sensing* (Centre for Remote Imaging; Sensing, and Processing, National University of Singapore, Singapore), Vol. I, pp, 59–64.

Huete, A. R. 2004. Remote sensing of soils and soil processes. In: *Remote sensing for Natural Resource Mangement and Environment Monitoring. Manual of Remote Sensing*, edited by S. L. Ustin 3rd edition, Volume 4 (John Wiley & Sons, Inc, Hoboken, NJ, USA), pp. 3–52.

Hunt, E. R. Jr., Daughtry, C. S. T., McMurtrey, J. E., Walthall, C. L., Baker, J. A., Schroeder, J. C. and Liang, S. 2002. Comparison of remote sensing imagery for nitrogen management. In: *Proceedings of the Sixth International Conference on Precision Agriculture and Other Precision Resources Management*, edited by P. C. Robert, R. H. Rust and W. E. Larson (ASA-CSSA-SSSA, Madison, WI, USA), CD-ROM.

Hunt, E. R. Jr., Daughtry, C. S. T., Walthall, C. L., McMurtrey, J. E. and Dulaney, W. P. 2003a. Agricultural remote sensing using radio-controlled model aircraft. In: *Digital Imaging and Spectral Techniques: Applications to Precision Agriculture and crop Physiology*, edited by T. VanToai, D. Major, M. McDonald, J. Schepers and L. Tapley (ASA-CSSA-SSSA, Madison, WI, USA), pp. 191–199. ASA Special Publication 66.

Hunt, E. R. Jr., Everitt, J. H., Ritchie, J. C., Moran, M. S., Booth, D. T., Anderson, G. L., Clark, P. E. and Seyfried, M. S. 2003b. Applications and research using remote sensing for rangeland management. Photogrammetric Engineering & Remote Sensing **69**(6), 675–693.

Inoue, Y., Morinaga, S. and Tomita, A. 2000. A blimp-based remote sensing system for low-altitude monitoring of plant variables: A preliminary experiment for agricultural and ecological applications. International journal of Remote Sensing **21**(2), 379–385.

Lu, Y.-C., Daughtry, C., Hart, G. and Watkins, B. 1997. The current state of precision farming. Food Reviews Intermational **13**(2), 141–462.

Lopez, J. R. and Robert, P. C. 2003. Use of unmanned aerial vehicles to gather remote sensing imagery for precision crop management. In *ASA-CSSA-SSSA Annual Meetings Abstracts November 2–6, 2003. Denver, Colorado* (ASA-CSSA-SSSA, Madison, WI, USA), CD-ROM.

Milton, E. L. 2002. Low-cost ground-based digital infra-red photography. International Journal of Remote Sensing **23**(5), 1001–1007.

Moran, M. S., Inoue, Y. and Barnes, E. M. 1997. Opportunities and limitations for image-based remote sensing in precision crop management. Remote Sensing of Environment **61**, 319–346.

Moran, S., Fitgerald, G., Rango, A., Walthall, C., Barnes, E., Bausch, W., Clarke, T., Daughtry, C., Everitt, J., Escobar, D., Hatfield, J., Havstad, K., Jackson, T., Kitchen, N., Kustus, W., McGuire, M., Pinter, P., Sudduth, K., Schepers, J., Schmugge, T., Starks, P. and Upchurch, D. 2003. Sensor development and radiometric correction for agricultural applications. Photogrammetric Engineering & Remote Sensing **69**(6), 705–718.

Pierce, F. J. and Nowak, P. 1999. Aspects of precision agriculture. Advances in Agronomy **67**, 1–85.

Pinter, P. J. Jr., Hatfield, J. L., Schepers, J. S., Barnes, E. M., Moran, M. S., Daughtry, C. S. T. and Upchurch, D. R. 2003. Remote sensing for crop management. Photogrammetric Engineering & Remote Sensing **69**(6), 647–664.

Quilter, M. C. and Anderson, V. J. 2000. Low altitude/large scale aerial photographs: A tool for range and resource managers. Rangelands **22**(2), 13–17.

Ritchie, S. W., Hanson, J. J. and Benson, G. O.1993. *How a corn plant develops, Special Report No. 48*. (Iowa State University of Science and Technology, Cooperative Extension Service, Ames, IA).

Robert, P. C. 2002. Precision agriculture: A challenge for crop nutrition management. Plant and Soil **247**, 143–149.

Rouse, J. W., Haas, R. H., Schell, J. A. and Deering, D. W. 1974. Monitoring vegetation systems in the Great Plains with ERTS. In: *Third Earth Resources Technology Satellite–1 Symposium. Volume I: Technical Presentations, NASA* SP−351, edited by S. C. Freden, E. P. Mercanti and M. Becker (National Aeronautics and Space Administration, Washington, DC), p. 309–317.

SAS Institute Inc. 1999. *SAS/STAT User's Guide*, Cary, NC.

Scharf, P. C. and Lory, J. A. 2002. Calibrating corn color from aerial photographs to predict sidedress nitrogen need. Agronomy journal **94**, 397–404.

Scharf, P. C., Schmidt, J. P., Kitchen, N. R., Sudduth, K. A., Hong, S. Y., Lory, J. A. and Davis, J. G. 2002. Remote sensing for nitrogen management. Journal of Soil and Water Conservation **57**, 518–524.

Shevell, S. 2003. *The Science of Color* 2nd Edition (Optical Society of America, Washington, DC, USA).

Verhoef, W. 1984. Light scattering by leaf layers with application to campy reflectance modeling: The SAIL model. Remote Sensing of Environment **16**, 125–141.

Wald, G. 1968. The molecular basis of visual excitation. Nature **219**, 800–807.

Waring, R. H., Law, B., Goulden, M. L., Bassow, S. L., McCreight, R. W., Wofsy, S. C. and Bazzaz, F. A. 1995. Scaling gross ecosystem production at Harvard Forest with remote sensing: A comparison of estimates from a constrained quantum-use efficiency model and eddy correlation. Plant, Cell & Environment **18**, 1201–1213.

Yang, C., Everitt, J. H., Bradford, J. M. and Esccibar, D. E. 2000. Mapping grain sorghum growth and yield variations using airborne multispectral digital imagery. Transactions of the ASAE **43**(6), 1927–1938.

Zarco-Tejada, P. J., Rueda, C. A. and Ustin, S. L. 2003. Water content estimation in vegetation with MODIS reflectance data and model inversion methods. Remote Sensing of Environment **85**, 109–124.